Experiment and Analysis of a Hybrid Composite Post-tension Plate Girder

Sahib Al Mustawfi, Nor Azizi Safiee*, Nabilah Abu Bakar, Izian Abd Karim and Noor Azline Mohd Nasir

Department of Civil Engineering, Faculty of Engineering, Universiti Putra Malaysia, 43400 UPM, Serdang, Selangor, Malaysia

ABSTRACT

Steel plate girders have been employed as structural bridge parts since the 19th century. They are typically made up of built-up sections in the shape of I-beams. Web and flange plates withstand shear force and bending moment, respectively. However, plate girders are vulnerable to shear buckling. Shear buckling resistance is increased by adding reinforced vertical stiffeners and, in some cases, longitudinal stiffeners. Nevertheless, these stiffeners are sometimes not enough to prevent extreme shear buckling and only delay the shear buckling of slender web panels. This study investigated a hybrid composite post-tension (HCPt) plate girder by experiment and finite element (FE) analysis. The structural performance of the HCPt plate girder was tested using three specimens: a double-web plate girder, an in-fill concrete double-web plate girder and an in-fill concrete double-web plate girder with prestress. Results showed that the steel web filled with concrete presented preferable strength and behaviour to the hollow steel web because of the concrete in-fill. It had high load capacity, strength and ductility. The concrete in-fill prevented the steel web plate from buckling, and beams generally failed in a ductile manner. Applying prestressing techniques reduced deflection under external loads, increased the load-carrying capacity and enhanced its flexural behaviour by 126% compared to the double web plate girder. The failure mode was changed from web shear buckling in a double web girder to bending in a hybrid composite plate girder, with an improvement of web shear buckling by 88%. The FE analysis result showed excellent consistency with the experimental result.

Keywords: Composite steel concrete prestress girder, finite element analysis, flexural strength, in-fill concrete, tendon, web distortion

INTRODUCTION

Since the 19th century, steel plate girders have been used as structural bridges and large structures to meet the design requirements associated with heavy loads and long spans (Barker & Puckett, 2013; Ismail et al., 2023). The plate girders are typically built-up sections in the form of I-beams made of a combination of steel plates (Aghayere & Vigil, 2020). In addition, plate girders offer not only a larger span but also provide more load capacity. Given its efficient section rigidity, the I-shaped plate girder is commonly utilised as a flexural component (Sim, 2019). Plate girders are primarily designed with very deep and slender webs to minimise the required area for flanges and realise a high strength-to-weight ratio; the web panel resists a significant portion of the shear force in a plate girder, which results in slender web plates that are prone to shear buckling (Ali & Elgammal, 2023; Azmi et al., 2017; Chacón et al., 2011; Ghadami & Broujerdian, 2019; Sim, 2019). To remediate this problem, reinforced vertical and longitudinal stiffeners are added to raise the shear buckling strength and improve moment capacities (Luo et al., 2023). In some cases, stiffeners are not enough to resist high shear and only delay shear buckling of the slender web panels (Al-Azzawi et al., 2020; Azmi et al., 2017; Basher et al., 2011; Frankl, 2017; Yuan et al., 2019).

Incorporating composite-based systems into steel components has been practically idealised by including in-fill concrete. A number of previous researchers used in-fill concrete as an alternative way to improve the buckling issue in slender webs. Cho et al. (2018) investigated the flexural strength of a concrete-filled steel tube composite girder using a simple equation for negative and positive bending moments. The wide flange plates and a thin-walled corrugated steel web produce corrugated steel web girders (Ghanim et al., 2021). The shear buckling performance was investigated by Wang et al. (2018) by using a trapezoidal profile web girder through experimental work and finite element (FE) analysis. The results showed that no global member buckling occurred for flat plate and corrugated web, which was attributed to the flexural stiffness of concrete-filled tubular flanges. The concrete-filled steel tube was examined under shear buckling behaviour by nonlinear FE analysis (FEA). The shear buckling test result indicated enhanced shear buckling resistance compared to the traditional plate girder (Sim, 2019). A simply supported plate girder with a curved concrete-filled tubular flange was investigated analytically and experimentally; the results showed that the rising number of transverse stiffeners enhanced the load-carrying capacity and most minor lateral displacement (Gao et al., 2020).

The growing demand for strengthening bridges and steel structures is due to the increasing load demand during its service life (Kazem et al., 2018). Recent research has focused on prestressed composite girders, active techniques for achieving serviceability because they are efficient for deflection control, strength improvement, and the ability to span longer lengths (Lorenc & Kubica, 2006). External prestressing is frequently used

to strengthen new or present steel plate girder bridges because of its effectiveness and economic feasibility (Ahn et al., 2010). Prestressing techniques have been applied not only to reinforced concrete structures but also to steel plate girders. Amongst the applications in which prestressing techniques were used were in I-shaped cross-sectional steel beams, which were utilised as roof structural elements (Belletti & Gasperi, 2010). Moreover, a steel plate box girder was tested under flexural behaviour and finite element to verify the effectiveness of the prestressing technique; the result showed enhancement proportion by the improvement in the rate of the applied external load (Kambal & Jia, 2018). The request for horizontal members with long spans and floor height reduction has been raised in large-scale architectural buildings (Lee et al., 2015).

Therefore, several attempts have been made to build long-range steel–concrete composite members (Heo et al., 2007). Prestressed composite girders with corrugated webs were examined by experimental work, and the mechanics of horizontal shear transmission between steel girders and concrete were explored; the outcomes demonstrated excellent flexural performance in comparison with that of the non-prestressed specimen (Lee et al., 2015). In addition, prestressed concrete-filled steel tube truss girders were studied by both FEAs and experimental tests; the outcome showed increased flexural strength as the prestress level or shear-span-to-depth ratio rose (Huang et al., 2017). The mechanical properties of the composite box girder with corrugated steel web were analysed through two rounds of tensioning of internal prestressed tendons. An FE model was established based on experimental, theoretical, and numerical results. The findings indicated that the prestress of the concrete floor could be efficiently transferred to the concrete roof during tensioning, while the corrugated steel web mainly transferred the force of the section (Zhang et al., 2023).

This paper presents a study of the efficiency of a newly proposed hybrid composite post-tension (HCPt) plate girder, as shown in Figure 1, which comprises enhanced steel and concrete with prestressing. The arrangement of this plate girder is expected to produce a long span, thereby strengthening the web resistance against shear buckling, reducing the deflection and enhancing the flexural resistance. Combining steel and concrete with prestressing will improve the plate girder's performance. The performance of the HCPt plate girder was assessed using experimental and FEA approaches.

MATERIALS AND METHODS

Description of the HCPt Plate Girder System

The HCPt plate girder was designed based on BS 5950-1:2000 (BS5950, 2008) and BS 8110-1: 1997 (BS8110, 1997). The design was created so the HCPt would fail in the web shear buckling mode. Three specimens were developed to test the performance of the girder and portray the different effects of significant design parameters. The first specimen (FS1)
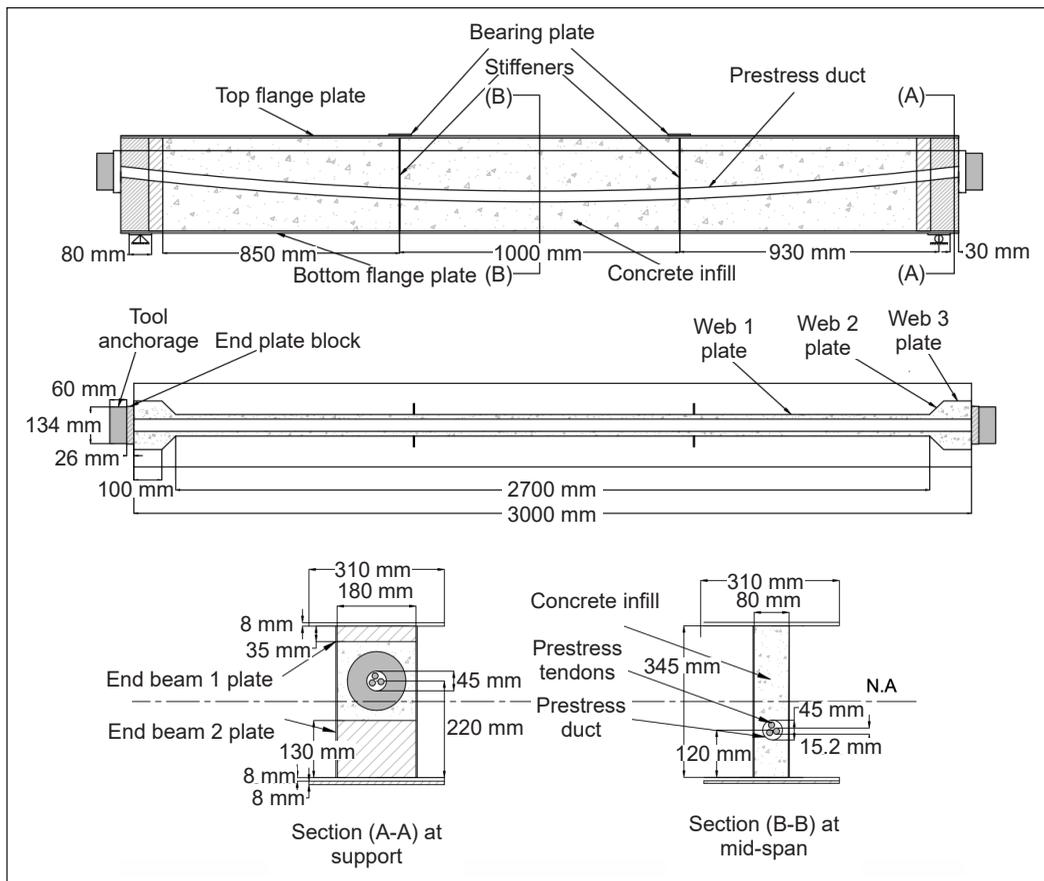
Figure 1. HCPt plate girder

was designed with double webs (the control), the second specimen (FSC2) had concrete in-fill between the double webs, and the third specimen (FSCP3) had concrete in-fill double webs with prestressing steel.

The HCPt plate girders were fabricated using mild steel plates of grade S275. Figure 1 shows the side view, top view and a related cross-section taken at support and mid-span. Flat steel plates with two different thicknesses (2.5 mm for web and stiffener; 8 mm for flange and bearing plate) were used with continuous fillet welds to connect them. The main dimensions remained fixed for all the specimens' girders: span length, L = 3000 mm; web thickness, t_w = 2.5 mm; web depth d = 345 mm; flange width, b_f = 310 mm; flange thickness, t_f = 8 mm; stiffener thickness, t_s = 2.5 mm; web slenderness ratio, d/t_w = 138; L/d = 8.7. Two vertical stiffeners were placed at a point of load application, as illustrated in Figure 2. Grade 40 MPa was used for concrete in-fill. The steel strand comprised three tendons, each having seven wires of 15.24 mm with a 5 m length and a strength of f_{pk} = 1860 MPa (low relaxation).
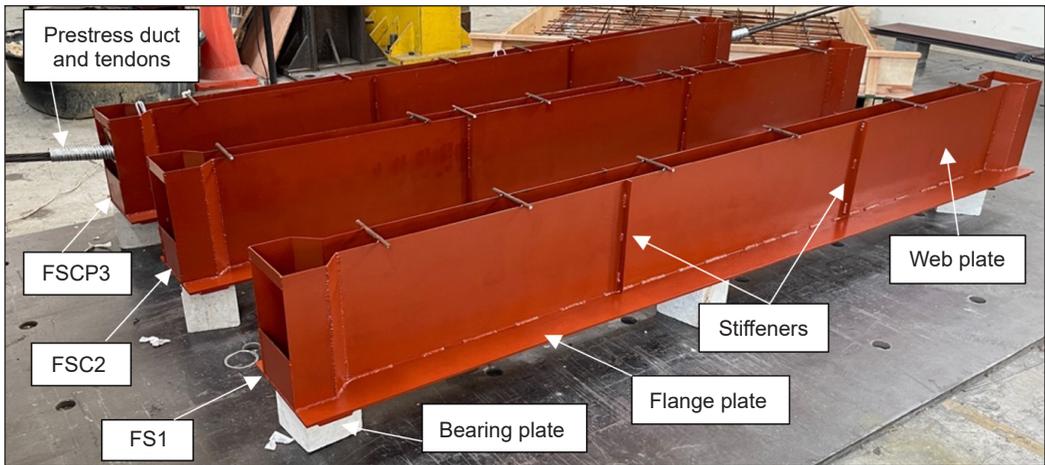
Figure 2. HCPt plate girder specimens before in-fill concrete casting and the top flange

Experimental Investigation

In this study, three plate girder specimens were prepared, named FS1, FSC2, and FSCP3. The description of each is presented in Table 1.

Material Properties

The characteristics of the main materials, steel and concrete, were evaluated by performing the appropriate test. Steel was tested via a tensile test, and concrete was tested for its mechanical properties.

Steel Properties

The basic stress–strain relationship of the steel plate of mild steel plates grade S275 was obtained by performing a tensile test on a coupon sample from the plate girder. A total of six coupons of two thicknesses (2.5 and 8 mm), as shown in Figure 3, were tested in tension. The tests were conducted

Table 1
Specimen description

Specimen	Description	Cross section
FS1	Double-web plate girder (Control specimen)	
FSC2	In-fill concrete double-web plate girder	
FSCP3	In-fill concrete double-web plate girder with prestress	

in accordance with the provisions of the Standard Test Methods for Tension Testing of Metallic Materials1 E8/E8M – 16a (ASTM, 2016). They were performed on a universal testing machine, INSTRON 3382, with 100 kN maximum capacity. The result of the

stress–strain of the 8- and 2.5-mm plates is shown in Figure 4. Table 2 presents their yield strength, ultimate strength and Young's modulus.

According to the tensile test results, the observed stresses at the yield point (f_y) and ultimate point (f_u) exceeded the nominal basic yield stresses (f_{yb}) and basic ultimate stresses (f_{ub}), which are equal to 275 MPa and 430 MPa, respectively. The nominal basic yield
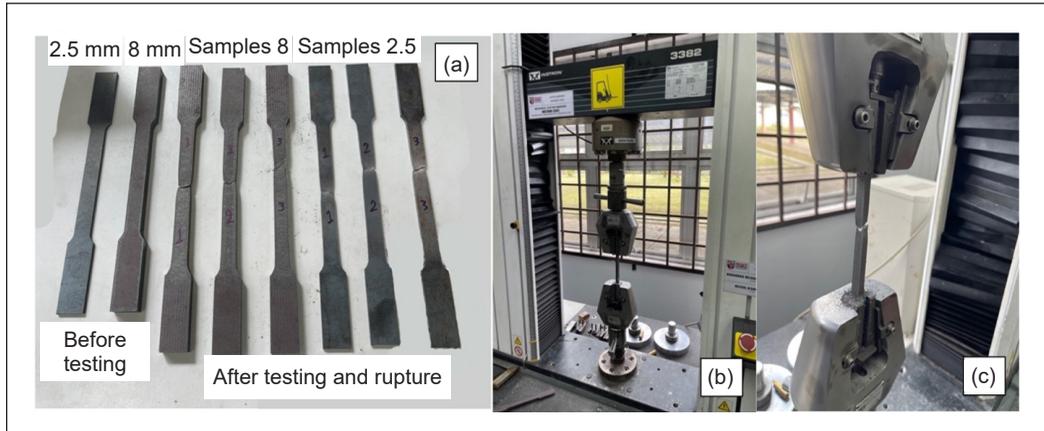

Figure 3. (a) Tension specimens before and after testing and rupture, (b) tensile testing machine and (c) sample after rupture

Table 2
The tensile test result of the 8 and 2.5 mm-thick steel plates

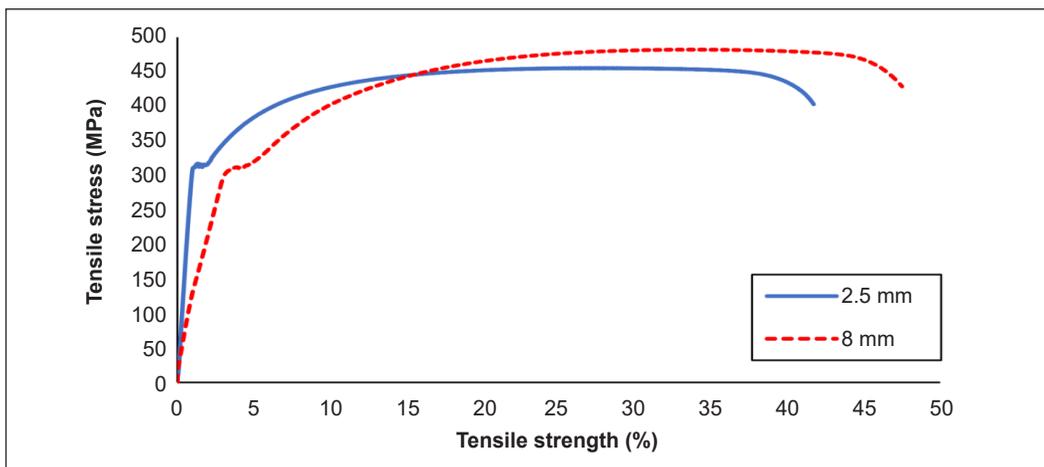| Plate thickness (mm)	Young's modulus (MPa)	f_y (MPa)	f_u (MPa)	Elongation (%)	Rupture strength (MPa)
8	205,000	312.3	481.48	33.2	383.7
2.5	210,000	320.6	455.14	28.12	382.2

Figure 4. Stress–strain curve for the 8 and 2.5 mm-thick steel plates

and ultimate stresses are average values for relative comparison and reference, but actual material qualities could vary. Material quality, production techniques, and impurities can cause variability. Some samples frequently demonstrate higher strength qualities than the nominal values. The thickness of the specimen used in the tensile test influences the observed stresses; thinner specimens may exhibit higher stresses due to thickness effects. Metals often exhibit plasticity and strain hardening, meaning they can deform and maintain strength after the initial yield point. This behaviour can result in observed ultimate stresses greater than nominal ones. The coupon test samples were cut using a CNC laser, producing a very high amount of heat. This amount would change the steel's properties by tempering it. The 8 mm-thick steel had a lesser yield strength than the 2.5 mm-thick steel because the lower thickness of 2.5 mm steel gained heat faster than the thicker steel of 8 mm. It changed the properties of the 2.5 mm steel, which gained higher yield strength than the 8 mm steel.

The prestressed steel tendons consist of seven high-strength steel strands of f_{pk}=1860 MPa low-relaxation steel with 15.24 mm diameter and 140 mm^2 cross-section. The Young's modulus was 195 GPa, and the tendon was steel grade 270. The nominal weight is 1100 kg/1000m, and the minimum elongation is 3.5 %. The specification details of the prestressing tendon were obtained from the manufacturer of a tendon (Southern Steel Berhad, 2022), and it complies with the standard (ASTM A416/A416M-16a).

Concrete Properties

Two different batches of concrete of grade 40 MPa were prepared for each plate girder. The compressive strength was investigated using six concrete cubic specimens with a size of 100 mm × 100 mm × 100 mm at 7 and 28 days, and the splitting tensile strength was examined using three concrete cylinder specimens with 200 mm height and 100 mm diameter at 28 days of curing. The test procedure was in accordance with BS EN 12390-3(2009) (BSI, 2009) for the compressive strength and BS EN 12390-6(2009) (BSI, 2009) for the splitting tensile strength. Table 3 demonstrates the concrete mechanical properties.

Table 3
Mechanical properties of concrete

Mixes	Compressive strength (MPa)		Splitting tensile strength (MPa)
	7 days	28 days	28 days
M1	26.36	41.72	3.24
M2	27.63	38.51	2.56

The two mixes represented the properties of the concrete used as an in-fill to the hollow space between a pair of webs in a double web plate girder specimen. The result was based on two different batches, namely M1 and M2. The difference between these two batches was in the coarse aggregate source.

Fabrication of Specimens

Each specimen comprised separate structural steel plates, which were welded together to form plate girder. The plate girder was fabricated by assembling the different flange, web and stiffener plates by welding with continuous fillet welds. When welding the thin web plate (2.5 mm), sufficient care was taken to reduce the distortion caused by welding by providing lateral supports at specific intervals to prevent significant initial imperfections of the web, as shown in Figure 5. All specimens were tested by a four-point bending test (i.e., two-point loading at one-third span with simply supported end conditions). A simply supported state was adopted, and the support was placed 30 mm inwards from the ends of the beams at each end, as illustrated in Figure 6.

FSCP3 had steel stirrups for the end block prestress. The steel stirrups with 10 mm diameter, 140 mm length and 50 mm space, as illustrated in Figure 7, are made of steel grade S420. A prestressing company performed the prestress work for the FSCP3 specimen. Three prestressed steel tendons were used, as shown in Figure 8, each consisting of seven high-strength steel strands arranged in a curved profile shape. The steel tendon is placed in

Figure 5. Steel plate assembly process

Figure 6. Support conditions for the HCPt plate girder

the doubled plate girder web duct before concrete casting. The prestress duct used was a 45 mm round duct. In the 78 days following the concrete casting, the tendons were prestressed by a total jacking force from all tendons of 336 kN, with the prestressing force level taken as 50% of the yield strength of the tendon. Two hand tool anchorages, one on each end, with a diameter of 134 mm and a length of 60 mm, were used. The jack was connected to a hydraulic jack, as shown in Figures 9 and 10.
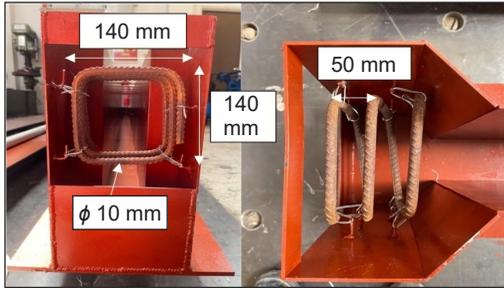

Figure 7. End block steel stirrups for the prestressed specimen (FSCP3)

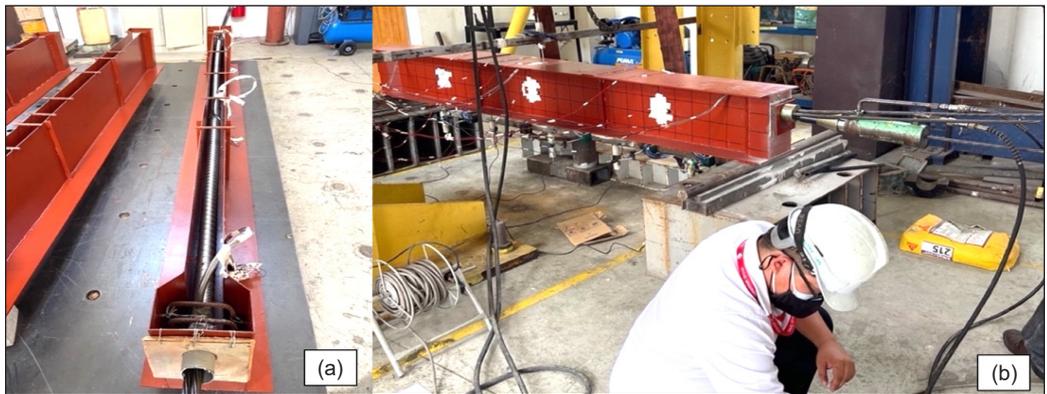*Figure 8.* Prestressed steel tendons are used

Figure 9. FSCP3 sample: (a) prestressing duct and tendons before concrete casting and (b) prestressing progress by using a prestress jack

Figure 10. (a) Prestress mono jack and (b) hydraulic jack

Test Setup

Different gauges were used to record the strain, load, displacement and prestress jack force, such as strain gauge, load cell and LVDT, as illustrated in Figure 13. All the data were recorded on a computer using a data acquisition system. A strain gauge of size 5 mm length was used to measure strain in steel components, in plate girder and prestressing tendon, as shown in Figures 11(a) and 11(b). A strain gauge of 30 mm long was used for the concrete; two strain gauges were used for each sample situated on the top surface of the concrete at mid-span, as shown in Figure 11(c). The specimens' vertical deflections were measured using five LVDTs attached to the centre of the bottom flange, as demonstrated in Figure 12. One load cell with a maximum capacity of 1000 kN, located at mid-span, was used. The load was sourced from a hydraulic manual jack. All readings from the strain gauges, load cell and LVDT were recorded at 30 s with 10 kN load-interval increments until failure. For specimen FSCP3, the testing is divided into two steps: first, applying tension to tendons; second, starting the test directly to avoid any losses in prestress tendons.

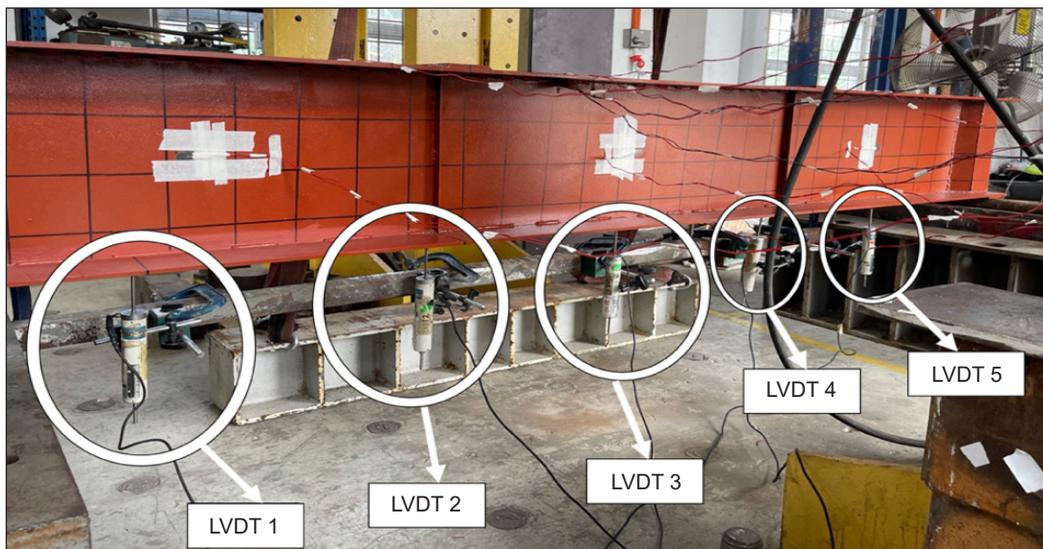*Figure 11.* Strain gauge attached to (a) steel plate girder, (b) prestress tendon and (c) concrete

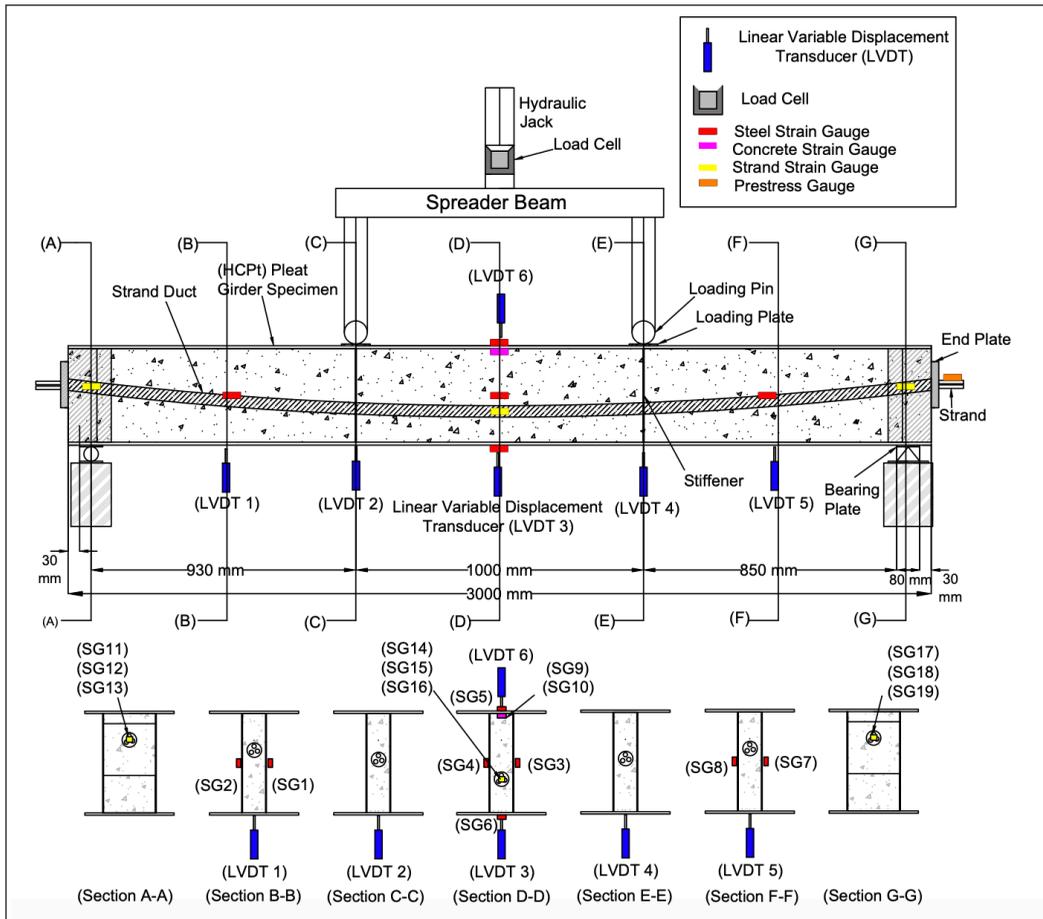*Figure 12.* LVDTs affixed in the specimen

Figure 13. The placement of measurement gauge on plate girder specimen

FE Modelling

The numerical study used the FE software Abaqus (Manual, A. U., 2020). The experimental results for FS1, FSC2 and FSCP3 were subsequently used to validate the FE models. The selection and type of element used in developing the geometrical model are shown in Table 4 and Figure 14. The overall element mesh size was 40 mm with an aspect ratio of mesh element = 1; the aspect ratio is the ratio between an element's longest and shortest edge. The command merge in FE Abaqus was used to model the welding effect. The merge command in Abaqus is primarily used to merge nodes close to each other to eliminate redundancy in the model. The material properties of the steel plate of the flange, web, bearing plate, end plate, bar and stirrup are shown in Table 5. The properties of the steel tendon material for the elastic and plastic behaviours are provided in Table 6. For the concrete, with two different batches for the FSC2 model and the FSCP3 model, concrete damage plasticity was used to define the concrete properties. Abaqus's concrete damage

plasticity model provided a general property for modelling concrete in structure solid type. According to Mander et al. (1988) and GabrielaSanMartín (2008), a concrete material can be characterised by compressive strength f_c, ε_c strain at f_c and ε_u ultimate concrete strain capacity. Table 7 provides the details of the concrete properties. The constitutive relation for confined concrete using the concrete damage plasticity model assigned to the concrete material can simulate the confined effect by introducing the dilation angle. The concrete strength will increase when the pressure from the confined increases (Manual, A. S. U. S., 2012).

The FS1 model used a linear buckling step with imperfections to counter some imperfections caused by welding in the specimen. The FSC2 and FSCP3 models are analysed using dynamic and implicit types with a quasi-static application. The interaction between the concrete surface and steel surface and between the concrete surface and tendon surface was modelled using tangential and normal behaviour. A common assumption for

Table 4
Details for all parts of the plate girder model

Part	Element shape	Element type
Flange, web, and stiffener plate	Shell	S4R
Bearing plate, concrete, end block plate, tendon	Solid	C3D8R
Bar and stirrups	Wire	T3D2

Table 5
Material properties of the steel plates

Materials	Behaviour	Young's modulus (MPa)	Poisson's ratio	Mass density (tonne/mm)
Steel for bearing plate and end plate	Elastic	200,000	0.3	7.8 E-09
Steel-S275 for flange, web, and stiffener plates	Elastic	205,000 and 210,000	0.3	7.8 E-09
		f_y (MPa)		f_u (MPa)
	Plastic	2.5 mm 8 mm	2.5 mm	8 mm
		320.6 312.3	455.14	481.48
Reinforcement bar and stirrups	Elastic	200,000	0.3	7.8 E-09
	Plastic	Yield stress	Plastic strain	
		420	0	

Table 6
Material properties of the steel tendon

Materials	Behaviour	Young's modulus (MPa)	Poisson's ratio
	Elastic	195,000	0.3
Steel tendon		Yield stress	Plastic strain
	Plastic	1600	0
		1860	0.012

Table 7
Material properties of the concrete

Materials	Behaviour	Young's modulus (MPa)	Poisson's ratio	Mass density (tonne/mm)
Concrete	Elastic	31521.77898	0.2	2.4 E-09
Batches	Compressive strength (f_c) (MPa)	Strain ε_c	Strain ε_u	Tensile strength (f_t) (MPa)
M1	41 MPa	0.0019	0.0055	3.23
M2	38.5 MPa	0.0019	0.0055	2.56
Concrete damage plasticity				
Dilation angle	Eccentricity	F_{b0}/f_{c0}	K	Viscosity parameter
42	0.1	1.16	0.667	0.0001
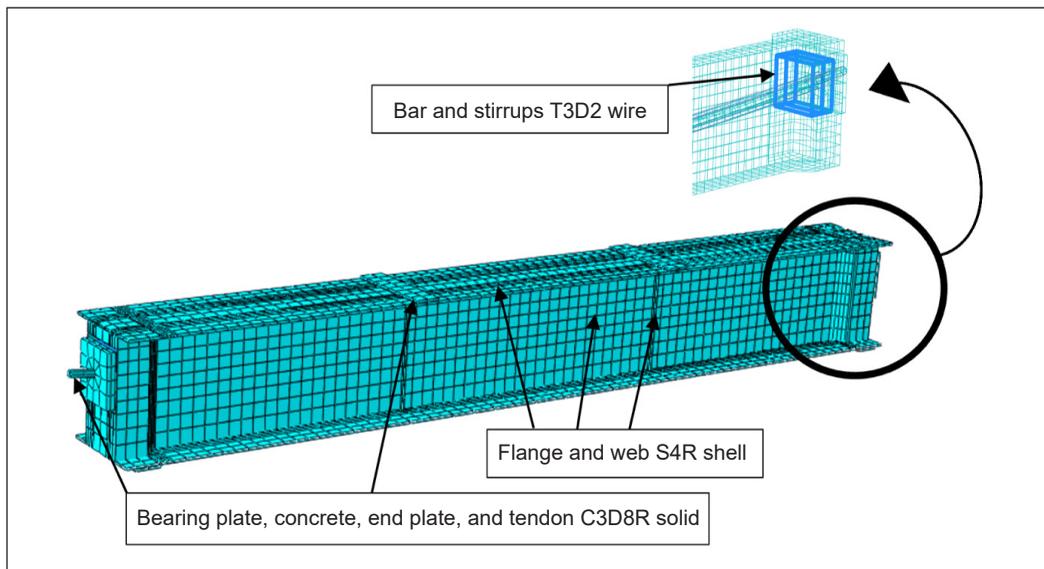
Figure 14. Typical FE mesh for the plate girder model

the coefficient of friction between concrete and steel is often 0.6 to 0.7. The tangential behaviour friction was characterised by a friction coefficient of 0.6, as recommended by Baltay and Gjelsvik (1990), Cho et al. (2018), and Rabbat and Russell (1985). The normal behaviour of pressure overclosure was hard contact, allowing separation. The boundary condition for all models was simply supported. The load for each model was demonstrated by displacement control. The prestress force is simulated by using prestress boundary conditions. The boundary conditions apply forces that simulate the effects of prestressing. The magnitude and direction of the prestress force are specified in terms of the type of applied force (stress) used in the selected region (tendon), and the stress value (Sigma33= 800 MPa) is predefined.

RESULTS AND DISCUSSION

Experimental Girder Result

This study tested three hybrid composite plate girder specimens (FS1, FSC2 and FSCP3) under flexural static load until failure. All specimens tested failed due to a combination of bending and shear buckling. The result of load and displacement was taken from the mid-span. The mid-span section was the most critical location in observing the girder behaviour. Figure 15 shows the load–displacement of all specimens. The loading was applied gradually in static by two-point loads. In the first stages of loading, all the girders exhibited positive bending, with only slight deflection seen at the mid-span.

From Figure 15, the first specimen FS1 demonstrated web shear buckling at a load of 288 kN. Moreover, right after that, at an identical magnitude of load, the failure of the specimen occurred. The maximum load corresponds to 5.4 mm displacement when the web buckling happens. At this stage, the FS1 specimen reached the ultimate state. Hence, the shear resistance loss in the web and plate girder collapsed. The second specimen was FSC2; the web shear buckling occurred at a load of 520 kN with 10.5 mm displacement; here, the specimen was able to resist the applied load after the web buckling occurred. Web buckling occurred in a later stage compared to specimen FS1 due to the presence of concrete within the web, which provides more resistance to lateral movement. The load then increased until reaching the maximum of 623.32 kN, corresponding to 18 mm displacement, and reduced afterwards. This phenomenon indicated that the plate girder reached the ultimate load and failed in bending. Compared with FS1, the improvement in maximum load was 116.43%, and the displacement increased by 12.6 mm.
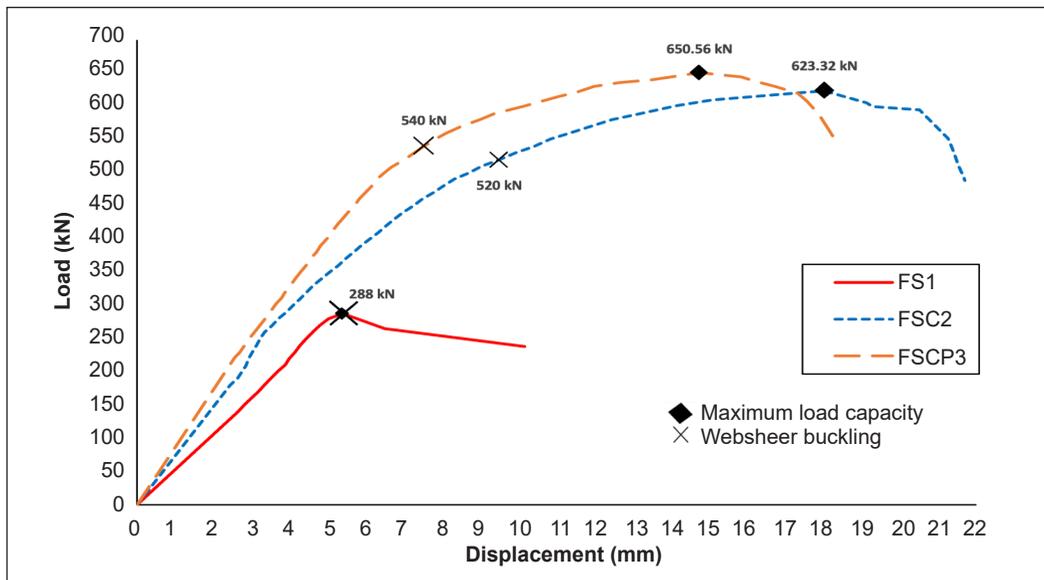

Figure 15. Experimental load–displacement curve for FS1, FSC2 and FSCP3 specimens at mid-span

This enhancement was contributed to by concrete in-fill that produced composite plate girder members that showed improved ductility. The concrete in-fill had a high flexural load capacity, good structural performance, high web buckling resistance strength, stiffness and energy dissipation ability. In this respect, the concrete in-fill was confined by the surrounded steel plate, resulting in a tri-axial state of compression that increased the strength and strain capacity of the concrete; beams generally fail in a very ductile way (Chen & Wang, 2009; Cho et al., 2018; Hu et al., 2003; Kim, 2005; Lu et al., 2009). The effect of the composite plate girder with concrete in-fill was evident at the delaying stage in comparison to FS1 when web shear buckling of the FSC2 specimen occurred at the load of 520 kN, corresponding to 9.5 mm displacement; FSC2 kept resisting until the ultimate load. This result indicated that the improvement in shear buckling resistance compared with FS1 was 80% by delaying the occurrence of web buckling. In particular, when subjected to flexural loading conditions, the crushed in-fill concrete remained confined within the steel, providing energy dissipation with delayed resistance degradation (Cho et al., 2018). Shao and Wang (2017) stated that concrete in-fill enhanced the global stability of the web's flexural strength and local shear buckling.

In the third specimen, FSCP3, the first displacement resulted from the mid-span at the prestress tensioning stage. When tension force was applied to tendons, the upward displacement was −0.1 mm from the experimental work. Web shear buckling occurred at 540 kN with 7.5 mm displacement, and the applied load was sustained until reaching the maximum load of 650.56 kN, equivalent to 14.7 mm displacement before dropped, indicating that the plate girder attained its final state by demonstrated bending failure. In terms of maximum load, FSCP3 improved by 126% and 4.3% compared to FS1 and FSC2, respectively. FSCP3 had the highest stiffness compared with the two other specimens; however, it has less displacement than FSC2. This result was due to the presence of prestress concrete in-filled by producing a prestress composite plate girder. The enhancement of FSCP3 in shear buckling occurrences compared with FS1 was 88%. Unlike the non-prestressed specimen FSC2, the prestressed specimen FSCP3 significantly increased initial stiffness and ultimate strength.

Figure 16 shows the labelling of the plate girder web panel for the schematic referring in the discussion. The FS1 specimen failed by web shear buckling, and the FSC2 and FSCP3 specimens failed by bending. For the FS1 specimen, at loading 288 kN, a diagonal-shaped buckling in the thin web was visible in web plates starting in web panels numbers 3 and 6 at the upper corner of the roller support region, as shown in Figure 17 for the FS1 specimen. At this stage, the FS1 specimen reached the maximum web shear buckling resistance, and the plate girder failed in web shear buckling. A similar observation was obtained at loadings of 520 kN and 540 kN for FSC2 and FSCP3 specimens, respectively. A slight effect from web buckling was exhibited in web panels numbers 1, 3, 4, and 6, with

two parallel diagonal-shaped buckling lines spaced 20 cm apart, as shown in Figure 18. The load continued to increase after the web buckling occurred; the load increased until reaching the maximum load of 623.32 kN for the FSC2 specimen and 650.56 kN for the FSCP3 specimen, which indicated that the plate girder failed in bending.

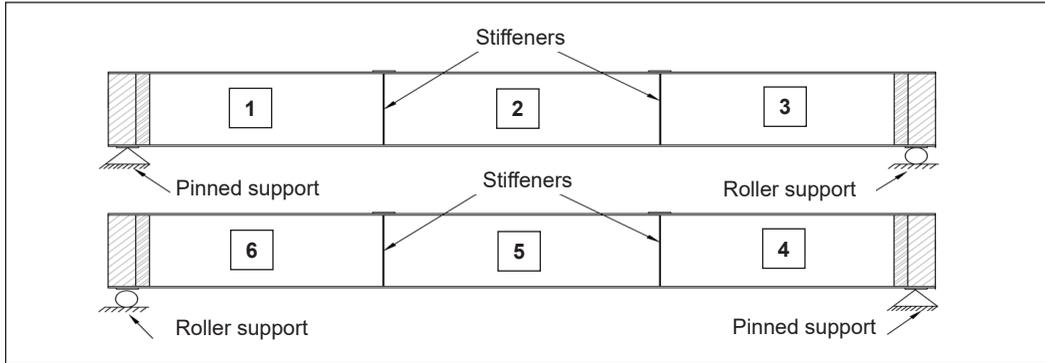The FSCP3 model fails at 650.56 kN, and the FSC2 model fails at 623.32 kN, which means an enhancement of 4.4% has been achieved; however, the displacement is decreased

Figure 16. Web panel numbering for double web

Figure 17. Diagonal-shaped buckling at web plates near the roller support for the FS1 specimen
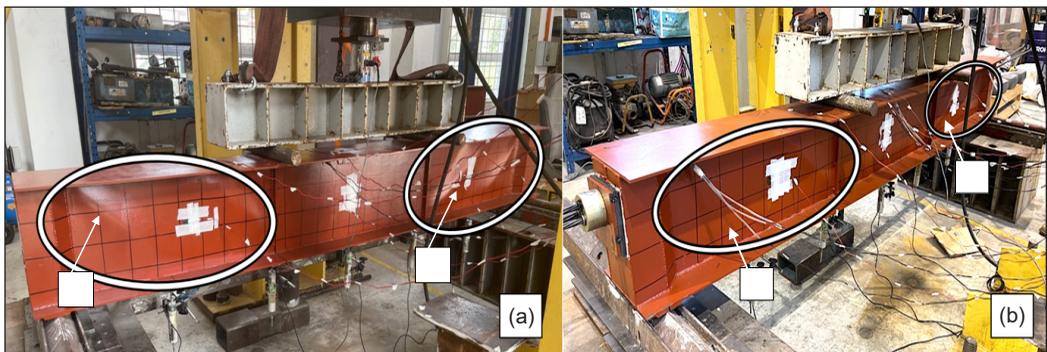
Figure 18. Diagonal-shaped buckling for (a) FSC2 and (b) FSCP3 specimens

by 18% due to the prestress improvement. Prestressing effects impact it; the high initial forces of composite prestressed plate girders incorporate prestressing tendons that introduce high initial compressive forces in the concrete. These forces affect the structural response and lead to a decrease in failure displacement. An investigation has been carried out for various HCPt plate girders FS1, FSC2 and FSCP3 to find out the effect of each part on the HCPt plate girder; the effect percentage had been reviewed for each part, whether it was effective or ineffective.

Validation of FE Models via Experiment

FE models were developed using the FEA Abaqus software. The models developed replicated the experimental specimens in terms of their geometric details. The outcomes obtained from the FEA were compared with the experimental results in Table 8 and Figure 19 to validate the accuracy and reliability of the developed FE model.

The FEA results for the FS1 model showed good agreement with similar pattern plotting to experimental results, indicating excellent accuracy. For the FSC2 model, both curves had a good agreement until up to 360 kN and more scatter at load between 360 kN and 603 kN before closely agreeing after load of 604 kN. FE model of FSC2 was stiffer compared to the experimental. The differences in the agreement could be due to the fact that the model consisted of steel and concrete, and concrete is a non-homogeneous material. The FSCP3 model curve was in good agreement with the experimental result. The failure mode for the
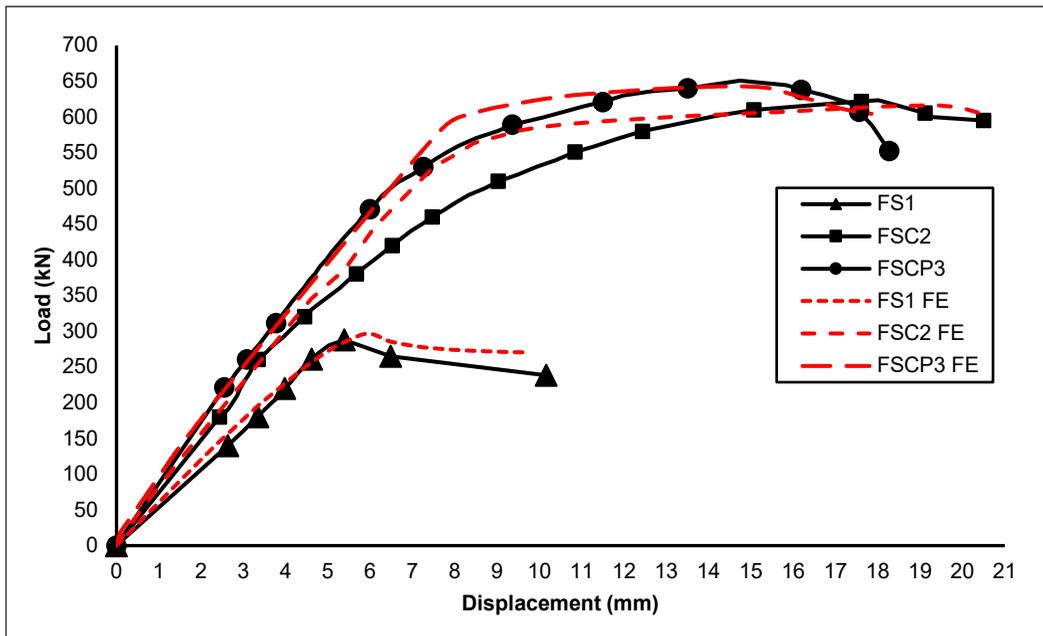

Figure 19. Load–Load-displacement curve for FS1, FSC2 and FSCP3 specimens at mid-span for both FEA and experiment

three FE models was the same as the experimental mode, which portrayed web buckling and bending failure modes. The FE models could predict the load-deflection response and strength of the hybrid composite plate girders with acceptable accuracy and failure mode.

Table 8
Comparison results obtained by FEA and the experimental

Model	Maximum load capacity		%	Maximum displacement		%
	Experiment	FEA		Experiment	FEA	
FS1	288 kN	297 kN	3%	5.4 mm	5.98 mm	9%
FSC2	623.32 kN	616 kN	1.2%	18 mm	19.1 mm	6%
FSCP3	650.56 kN	642.7 kN	1.2%	14.7 mm	14.6 mm	0.6%

The general failure mode comparison between the FEA and experiment for the FS1 specimen is depicted in Figure 20. Figure 21 compares the FE and experimental failure modes for FS1, which show identical modes in web shear buckling in web panel number 3. The degradation sign shown by web shear buckling occurred at load 288 kN for the experiment. At load 297 kN for FEA, a degradation sign was demonstrated by the web shear buckling line in the diagonal direction observed in web 3 and web 6. The web steel plate panel number 3 did not reach yield in FEA; the strain was 0.0008, and the maximum strain measured by the nearby strain gauge in the experiment was 0.00058, which was less than the yield strain, indicating that the steel was not achieved the yield strain capacity of 0.0015 for S275 when the web buckling occurred. as shown in Figure 21(a), web shear buckling near the roller support. Another sign of degradation was observed in one of the
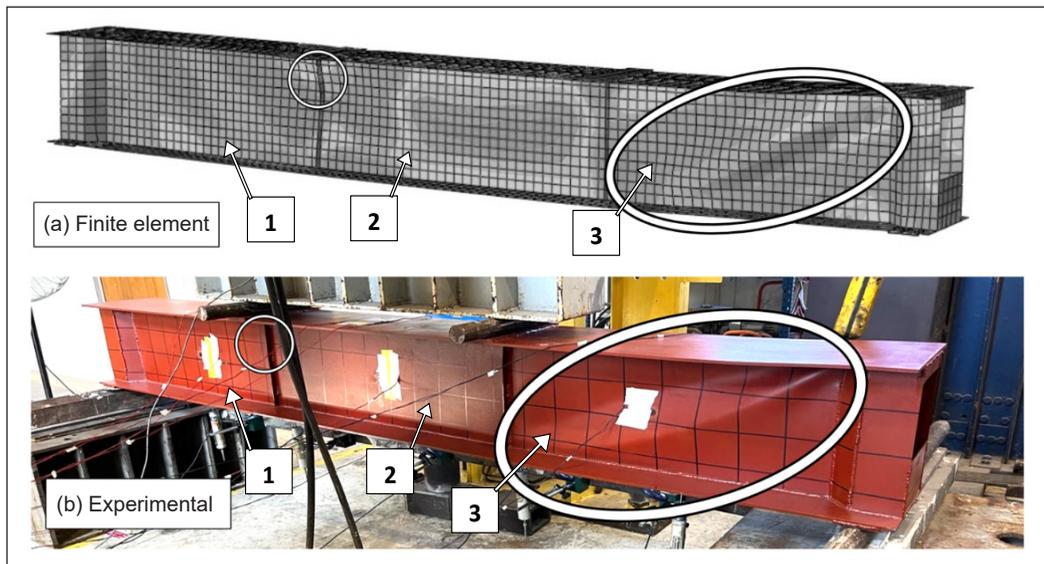

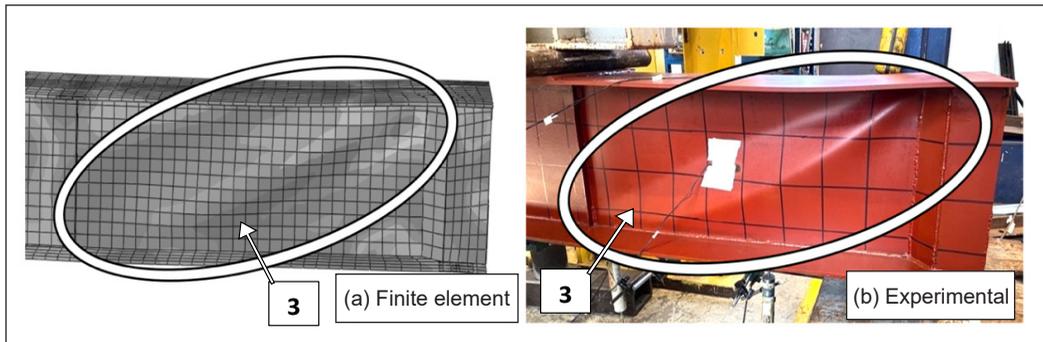*Figure 20.* General failure mode for FS1 in Abaqus FE

Figure 21. Identical failure mode exhibited in FS1 - web shear buckling near the roller support in both FEA and experimental
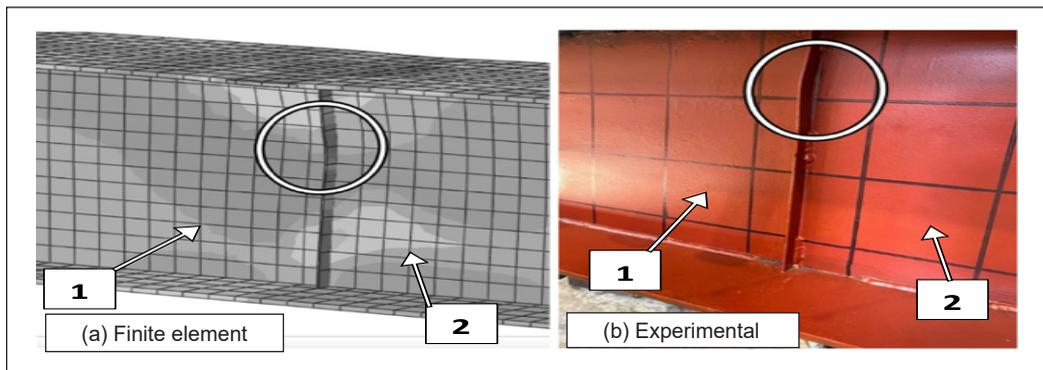

Figure 22. Degradation sign of web stiffeners in (a) FEA and (b) experiment

web stiffeners between panels 1 and 2 on one side only, as shown in Figure 22. The web stiffener buckling was observed to occur in an identical location for the FE and experimental for FS1, where it occurred at stiffeners between panels 1 and 2. The stiffener's failure was local due to the load applied at this point in the advanced stages of loading.

The failure sign in web buckling occurred in FSC2, demonstrated by both FEA and the experiment, as shown in Figure 23. Web shear buckling appeared at panels 1, 3, 4, and 6 of the girders in the experiment and FEA at 520 kN with 9.5 mm displacement and 533 kN with 7.4 mm displacement, respectively. In FEA, however, there are no signs of yielding for both the web and the flange. This discovery is consistent with the experimental results, which show no potential for yield occurring in the web, as seen by the maximum strain recorded at the web plate being 0.00105 for web panel number 3 and the maximum strain recorded at the bottom flange being 0.00105, less than the yield strain of steel, after reaching the ultimate load of 623.32 kN with 18 mm displacement for the experiment and 616 kN with 19.1 mm displacement for the FEA.

For experimental, there is no material yield observed as evidenced by the strain record for the web except the top flange and bottom flange, which reached yield with a recorded

maximum strain of 0.0017; however, in FEA, the web panels numbers 2 and 5 reached yield with a maximum strain of 0.0019, and the top and bottom flanges yielded with maximum strains of 0.0027 and 0.0054, respectively. It can be observed from Figure 19 that the stiffness for the FSC2 model in FEA is higher than the experimental result. It could be attributed to the fact that the material properties utilised in the FEA model are not an exact representation of the actual behaviour of the composite concrete plate girder. As a result, differences in stiffness may occur. Figures 24 and 25 show a close observation of web shear buckling in web panels 1 and 3 for FSC2 by experimental and FEA, which demonstrated the ability of the model to produce similar behaviour of girder as in the experiment.

For the FSCP3 model, in the transfer stage of tendon prestressing, the FE showed 0.14 mm upward deflection, as shown in Figure 26. Web shear buckling occurred in panels 1,
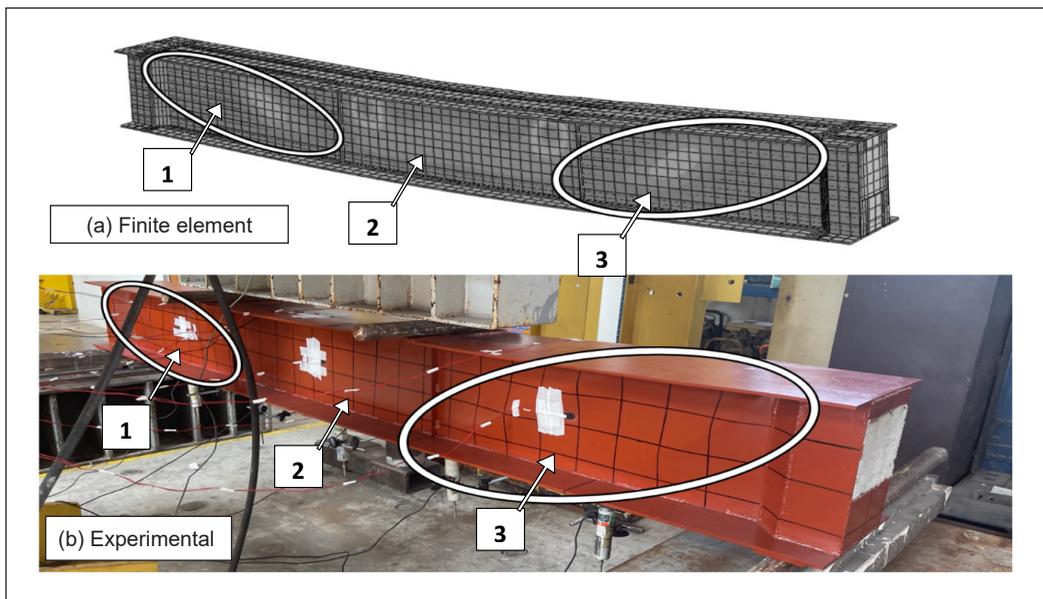

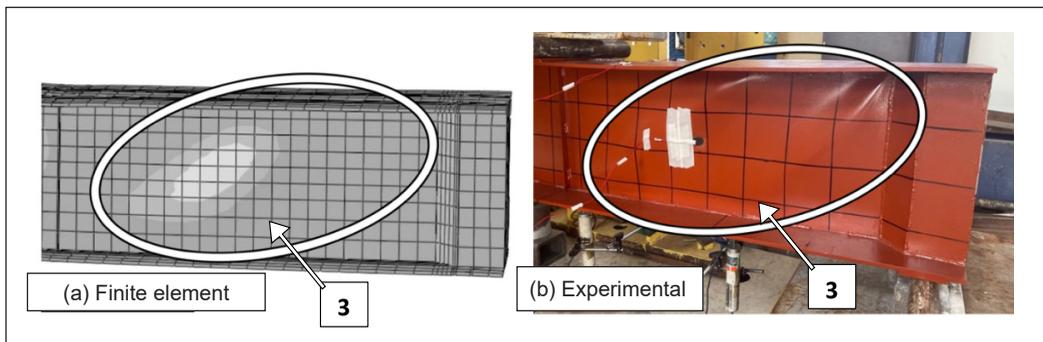*Figure 23.* Failure mode for FSC2 in (a) FEA and (b) experiment

Figure 24. Comparison between the failure mode for FSC2 in web share buckling near the roller support in (a) FEA and (b) experiment
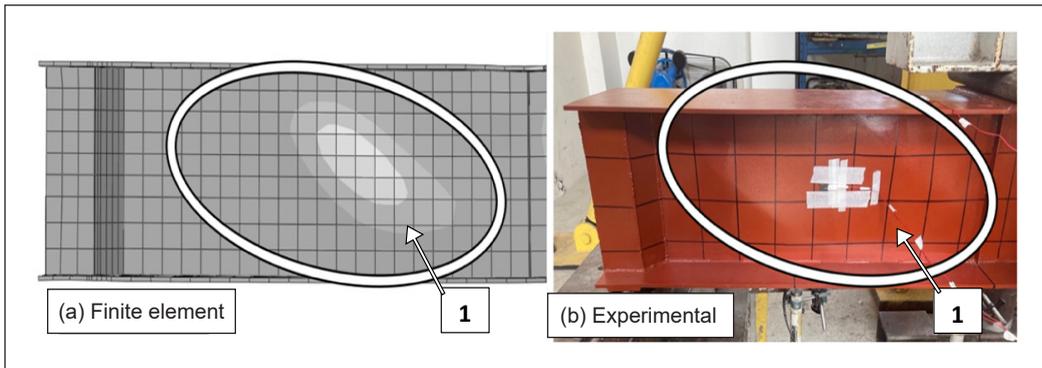
Figure 25. Comparison between the failure mode for FSC2 in web share buckling near the pinned support in (a) FEA and (b) experiment

3, 4, and 6 of the girders in FEA, which agree well with those observed in an experiment at loads of 540 kN and 564 kN, respectively, as shown in Figures 27 and 28. At this stage, the web was not observed to yield when web buckling occurred in both experimental and FEA, but the bottom flange began to yield when the load reached 588.8 kN with strain recorded at 0.0015 in FEA and 615 kN with strain recorded at 0.00154 in experimental. At the ultimate load, there is no yield recorded in the web plate in both experimental and FEA, except for the top and bottom flanges for both FEA and experimental, where the maximum strain for the top flange was 0.00152 and 0.002 demonstrated by experimental and FEA, respectively. The strain in the bottom flange was 0.0025 and 0.0027 in tension for experimental and FEA, respectively.

The failure modes observed by experimental and FEA are relatively identical to their corresponding experimental counterparts without remarkable differences. The FE models can predict the load-deflection response and strength of the HCPt plate girders with acceptable accuracy by demonstrating similar failure modes. This accuracy in the results enables the Abaqus finite element software to simulate other parameters' effects on the girder's behaviour.
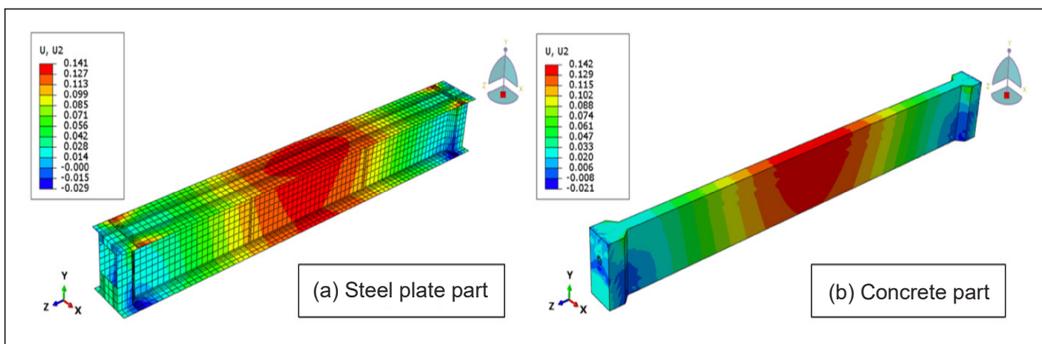

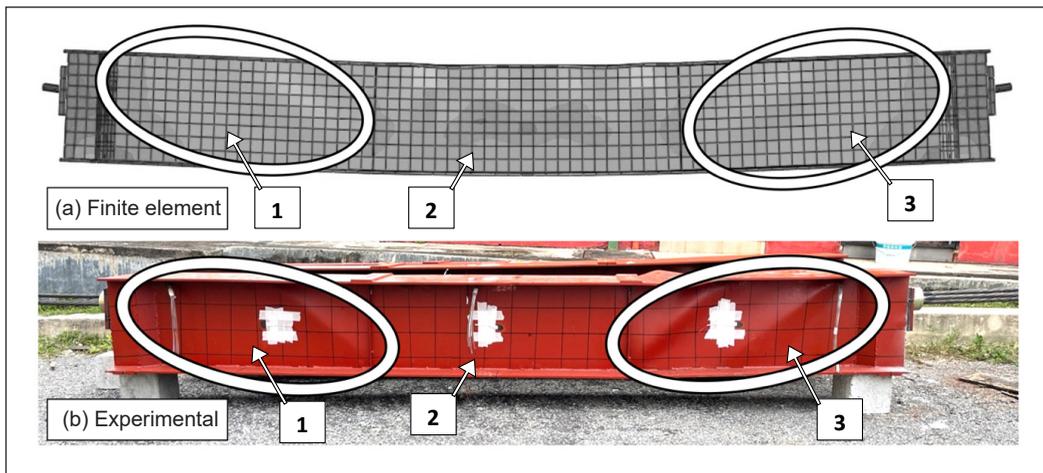*Figure 26.* FE model validation for the FSCP3 specimen: (a) steel plate part and (b) concrete part

Figure 27. Comparison of the general failure mode for FSCP3 in (a) FEA and (b) experiment
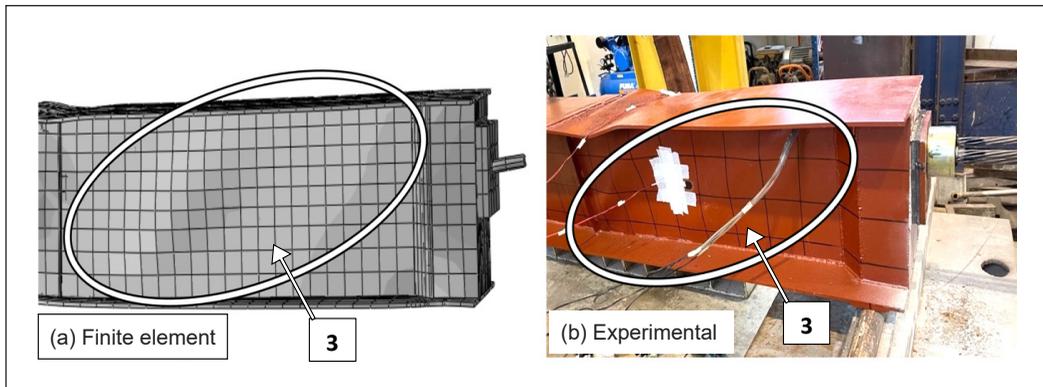

Figure 28. Comparison between the failure mode for FSCP3 in web share buckling near the roller support in FEA and experiment

CONCLUSION

The distortion and buckling web, as well as substantial deflection of long-span issues that occurred in traditional plate girder, has been addressed in this study by proposing a hybrid composite plate girder. This structural geometrical modification of the plate has been introduced by establishing the resistance of the web using the double web with in-filled concrete and enhanced with the internal prestressing tendon. The structural behaviour of this renowned plate girder was examined and investigated through experimental and finite element analysis using three specimens: FS1, FSC2 and FSCP3.

For flexural load capacity, in comparison to FS1, FSC2 produced 116.4%, and FSCP3 showed 126% improvement, respectively. In terms of displacement, FSCP3 exhibited a 20% reduction in displacement in comparison to FSC2.

The failure mode for FS1 was web shear buckling; those for FSC2 and FSCP3 were bending. The improvement in web shear buckling resistance produced by FSC2 and FSCP3 was 80% and 88%, respectively, in comparison to FS1.

For the FSC2 and FSCP3 specimens, the concrete in-fill is subjected to confinement effect by tri-axial compression, which is able to reduce the web buckling and improve the strength of the girder. The in-fill concrete was subjected to flexural load, and the concrete remained to provide high ductility and energy dissipation ability, delaying the failure of the girder.

FSCP3 produced the highest stiffness and load capacity compared to FS1 and FSC2, and it had less displacement than FSC2.

The model's FEA result showed excellent agreement with the experimental result. The failure modes simulated by the three models' FE were identical to the experimental work.

ACKNOWLEDGEMENTS

REFERENCES

Aghayere, A. O., & Vigil, J. (2020). *Structural steel design*. Mercury Learning and Information.

Ahn, J. H., Jung, C. Y., & Kim, S. H. (2010). Evaluation on structural behaviors of prestressed composite beams using external prestressing member. *Structural Engineering and Mechanics*, *34*(2), 247-275. https://doi.org/10.12989/sem.2010.34.2.247

Al-Azzawi, Z., Stratford, T., Rotter, M., & Bisby, L. (2020). A new design method for a novel FRP strengthening technique against shear buckling of steel plate girders. *Thin-Walled Structures*, *148*, Article 106611. https://doi.org/10.1016/j.tws.2020.106611

Ali, Y., & Elgammal, A. (2023). Compensating steel web-opened beams for the loss in cyclic shear capacity by longitudinal stiffeners. *Delta University Scientific Journal*, *6*(1), 123-134. https://doi.org/10.21608/dusj.2023.291030

ASTM. (2016). *E8/E8M-16a: Standard Test Methods for Tension Testing of Metallic Materials*. ASTM International.

Azmi, M. R., Yatim, M. Y. M., Esa, A., & Badaruzzaman, W. W. (2017). Experimental studies on perforated plate girders with inclined stiffeners. *Thin-Walled Structures*, *117*, 247-256. https://doi.org/10.1016/j.tws.2017.04.021

Baltay, P., & Gjelsvik, A. (1990). Coefficient of friction for steel on concrete at high normal stress. *Journal of Materials in Civil Engineering*, *2*(1), 46-49. https://doi.org/10.1061/(ASCE)0899-1561(1990)2:1(46)

Barker, R. M., & Puckett, J. A. (2013). *Design of Highway Bridges: An LRFD Approach*. John Wiley & Sons.

Basher, M., Shanmugam, N. E., & Khalim, A. R. (2011). Horizontally curved composite plate girders with trapezoidally corrugated webs. *Journal of Constructional Steel Research*, *67*(6), 947-956. https://doi.org/10.1016/j.jcsr.2011.01.015

Belletti, B., & Gasperi, A. (2010). Behavior of prestressed steel beams. *Journal of Structural Engineering*, *136*(9), 1131-1139. https://doi.org/10.1061/(ASCE)ST.1943-541X.0000208

BS5950. (2008). *BS 5950-1: 2000: Structural Use of Steelwork in Building. Part 1. Code of Practice for Design-Rolled and Welded Sections*. British Standard Institution. https://www.uceb.eu/DATA/CivBook/22.%20BS%205950%20Pt1%202000%20Steelwork%20Design.pdf

BS8110. (1997). Structural Use of Concrete, Part 1. Code of Practice for Design and Construction. BSI Knowledge. https://knowledge.bsigroup.com/products/structural-use-of-concrete-code-of-practice-for-design-and-construction?version=standard

BSI. (2009). BS EN 12390-3: 2009: Testing hardened Concrete. Compressive Strength of Test Specimens. BSI Knowledge. https://knowledge.bsigroup.com/products/code-of-practice-for-protection-of-below-ground-structures-against-water-from-the-ground?version=standard

Chacón, R., Bock, M., & Real, E. (2011). Longitudinally stiffened hybrid steel plate girders subjected to patch loading. *Journal of Constructional Steel Research*, *67*(9), 1310-1324. https://doi.org/10.1016/j.jcsr.2011.03.013

Chen, B. C., & Wang, T. L. (2009). Overview of concrete filled steel tube arch bridges in China. *Practice Periodical on Structural Design and Construction*, *14*(2), 70-80. https://doi.org/10.1061/(ASCE)1084-0680(2009)14:2(70)

Cho, J., Moon, J., Ko, H. J., & Lee, H. E. (2018). Flexural strength evaluation of concrete-filled steel tube (CFST) composite girder. *Journal of Constructional Steel Research*, *151*, 12-24. https://doi.org/10.1016/j.jcsr.2018.08.038

Frankl, B. A. (2017). *Buckling and Shear Capacity of Horizontally Curved Steel Plate Girders*. The University of Nebraska-Lincoln.

GabrielaSanMartín. (2008). *Technical Note Material Stress-strain Curves-csi*. Computers and Structures, Inc.

Gao, F., Zuo, G., Deng, L., & Yang, F. (2020). Flexural behaviour of horizontally curved I-girders with round concrete-filled tubular flange. *Journal of Constructional Steel Research*, *170*, Article 106090. https://doi.org/10.1016/j.jcsr.2020.106090

Ghadami, A., & Broujerdian, V. (2019). Shear behavior of steel plate girders considering variations in geometrical properties. *Journal of Constructional Steel Research*, *153*, 567-577. https://doi.org/10.1016/j.jcsr.2018.11.009

Ghanim, G., Baldawi, W. S., & Ali, A. (2021). A review of composite steel plate girders with corrugated webs. *Engineering and Technology Journal*, *39*(12), 1927-1938. https://doi.org/10.30684/etj.v39i12.2193

Heo, B. W., Kwak, M. K., Bae, K. W., & Jeong, S. M. (2007). Flexural capacity of the profiled steel composite beams-deep deck plate. *Journal of Korean Society of Steel Construction*, *19*(3), 247-258.

Hu, H. T., Huang, C. S., Wu, M. H., & Wu, Y. M. (2003). Nonlinear analysis of axially loaded concrete-filled tube columns with confinement effect. *Journal of Structural Engineering*, *129*(10), 1322-1329. https://doi.org/10.1061/(ASCE)0733-9445(2003)129:10(1322)

Huang, W., Lai, Z., Chen, B., & Yao, P. (2017). Experimental behavior and analysis of prestressed concrete-filled steel tube (CFT) truss girders. *Engineering Structures*, *152*, 607-618. https://doi.org/10.1016/j.engstruct.2017.09.035

Ismail, M. K., AbdelAleem, B. H., Hassan, A. A., & El-Dakhakhni, W. (2023). Prediction of tapered steel plate girders shear strength using multigene genetic programming. *Engineering Structures*, *295*, Article 116806. https://doi.org/10.1016/j.engstruct.2023.116806

Kambal, M. E. M., & Jia, Y. (2018). Theoretical and experimental study on flexural behavior of prestressed steel plate girders. *Journal of Constructional Steel Research*, *142*, 5-16. https://doi.org/10.1016/j.jcsr.2017.12.007

Kazem, H., Zhang, Y., Rizkalla, S., Seracino, R., & Kobayashi, A. (2018). CFRP shear strengthening system for steel bridge girders. *Engineering Structures*, *175*, 415-424. https://doi.org/10.1016/j.engstruct.2018.08.038

Kim, B. G. (2005). *High Performance Steel Girders with Tubular Flanges*. Lehigh University.

Lee, D. H., Oh, J. Y., Kang, H., Kim, K. S., Kim, H. J., & Kim, H. Y. (2015). Structural performance of prestressed composite girders with corrugated steel plate webs. *Journal of Constructional Steel Research*, *104*, 9-21. https://doi.org/10.1016/j.jcsr.2014.09.014

Lorenc, W., & Kubica, E. (2006). Behavior of composite beams prestressed with external tendons: Experimental study. *Journal of Constructional Steel Research*, *62*(12), 1353-1366. https://doi.org/10.1016/j.jcsr.2006.01.007

Lu, H., Han, L. H., & Zhao, X. L. (2009). Analytical behavior of circular concrete-filled thin-walled steel tubes subjected to bending. *Thin-Walled Structures*, *47*(3), 346-358. https://doi.org/10.1016/j.tws.2008.07.004

Luo, Z., Shi, Y., Xue, X., Zhou, X., & Yao, X. (2023). Nonlinear patch resistance performance of hybrid titanium-clad bimetallic steel plate girder with web opening. *Journal of Building Engineering*, *65*, Article 105703. https://doi.org/10.1016/j.jobe.2022.105703

Mander, J. B., Priestley, M. J., & Park, R. (1988). Theoretical stress-strain model for confined concrete. *Journal of Structural Engineering*, *114*(8), 1804-1826. https://doi.org/10.1061/(ASCE)0733-9445(1988)114:8(1804)

Manual, A. U. (2020). *Abaqus User Manual*. Abacus.

Manual, A. S. U. S. (2012). *Abaqus 6.11*. Abacus.

Rabbat, B., & Russell, H. (1985). Friction coefficient of steel on concrete or grout. *Journal of Structural Engineering*, *111*(3), 505-515. https://doi.org/10.1061/(ASCE)0733-9445(1985)111:3(505)

Shao, Y., & Wang, Y. (2017). Experimental study on static behavior of I-girder with concrete-filled rectangular flange and corrugated web under concentrated load at mid-span. *Engineering Structures*, *130*, 124-141. https://doi.org/10.1016/j.engstruct.2016.10.002

Sim, J. G. (2019). Shear buckling behavior of a plate composite girder using concrete-filled steel tube structures. *International Journal of Advanced Structural Engineering*, *11*, 377-384. https://doi.org/10.1007/s40091-019-00239-5

Southern Steel Berhad. (2022). *A Comparison of Specification for PC Strand*. Southern Steel Berhad. https://www.southsteel.com/upload/files/1691979722_Catalog_Spec._Rev_A._230811.pdf

Wang, Z. Y., Li, X., Gai, W., Jiang, R., Wang, Q. Y., Zhao, Q., Dong, J., & Zhang, T. (2018). Shear response of trapezoidal profiled webs in girders with concrete-filled RHS flanges. *Engineering Structures*, *174*, 212-228. https://doi.org/10.1016/j.engstruct.2018.07.025

Yuan, H., Chen, X., Theofanous, M., Wu, Y., Cao, T., & Du, X. (2019). Shear behaviour and design of diagonally stiffened stainless steel plate girders. *Journal of Constructional Steel Research*, *153*, 588-602. https://doi.org/10.1016/j.jcsr.2018.11.015

Zhang, Z., Zou, P., Deng, E.-F., Ye, Z., Tang, Y., & Li, F.-R. (2023). Experimental study on prefabricated composite box girder bridge with corrugated steel webs. *Journal of Constructional Steel Research*, *201*, Article 107753. https://doi.org/10.1016/j.jcsr.2022.107753